rinciples and Physical
Cliffs, N.J., 545 p.
circulation and inter-
y of Washington, Ph.D.

-mixed layer. J. Mar.

tructure in the vicin-
. Geophys. Res., 84:

in the Mediterranean.
- Woods Hole Oceano-

0) Comparison between
inertial oscillations.

Y. Thompson (1973) The
ophys. Fluid Dyn., 3:

uilibrium drift of the
: 281-297.
theory of the mixing
and oceanic turbu-

ment of pressure and
current systems, II.

e layer of frictional
Pap. Phys. Oceanogr.
r. Inst., 3: 1-100.
of an incompressible
387-397.
elds. Compt. Rend.

:s. Academic Press,

Course in Turbulence.

(1974) Modeling the
in Geophysics, 18A,

and prediction equa-
boundary layer. J.

CHAPTER 5

THE SURFACE HEAT AND MASS BALANCE

Gary A. Maykut

Department of Atmospheric Sciences/Geophysics
University of Washington
Seattle, Washington 98195

5.1 INTRODUCTION

Formation of a sea ice cover produces profound changes in the state of the atmosphere and ocean, primarily by altering the surface heat exchange. The high albedo of the ice and its insulation of the atmosphere from the underlying water give rise to a climate over the polar oceans that is more characteristic of the continental ice sheets than of a marine environment. Unlike the ice sheets, however, sea ice is only a thin veneer whose thickness and areal extent are sensitive to small changes in heat input. Variations in sea ice extent have the potential to amplify small changes in climate through a variety of positive feedback mechanisms (Kellogg, 1975), leading to their central role in several ice age theories (Brooks, 1949; Ewing and Donn, 1956, 1958; Budyko, 1966).

While an ice cover reduces the transfer of momentum from the air to the water, thermal processes associated with the growth and movement of the ice have the greatest impact on the ocean. In particular, evaporative heat losses and the absorption of solar radiation in the upper ocean are drastically reduced -- lack of light is the principal factor limiting biological activity beneath the ice in the Arctic Ocean. The ice also affects vertical motions in the mixed layer. Salt rejected by the growing ice forms cold dense brine which sinks, promoting convective overturning, and causing heat entering the mixed layer to be transported upward where it is rapidly lost to the ice. In contrast to the open ocean, no significant storage of heat occurs in the mixed layer beneath the ice pack.

Little is known about the heat and mass balance of ice-covered portions of the Southern Ocean due to inaccessibility and difficulties involved in making surface observations on the dynamic seasonal ice. In the north, however, measurements have routinely been carried out on most of the U.S. and Soviet drifting stations during the past few decades, producing substantial data on incident radiation, air and water temperatures, snowfall, winds, currents, and ocean structure in many parts of the Arctic Basin (Fletcher, 1965; Aagaard and Greisman, 1975). During the past few years data buoys have been deployed across much of the Arctic Basin and have begun to produce information on the large scale fields of atmospheric pressure, ice velocity, and surface temperature (Thorndike and Colony, 1980, 1981; Thorndike et al., 1982, 1983). A few similar buoys have also been deployed in the Antarctic (Ackley, 1981), but these have been generally limited to the somewhat atypical Weddell Sea and not to the seasonal ice which makes up most of the Antarctic ice pack. Despite recent attention to the marginal ice zone (MIZ) and areas of seasonal ice, our general understanding of interactions between the ice, the ocean, and the atmosphere is still largely based on what has been seen in the perennially ice-covered portions of the Arctic Basin. The applicability of such information to more dynamically active areas such as the MIZ and the antarctic ice pack is uncertain.

In the first part of this chapter we will review the various components of the surface heat balance and examine the relative magnitude of heat fluxes observed over the arctic ice pack. We will then describe the growth pattern and mass balance of a sea ice cover, consider different methods of predicting ice growth, and look at the sensitivity of sea ice to changes in climate. Finally, we will discuss the coupling between dynamic and thermodynamic processes, then estimate how thickness variations affect the regional heat exchange and ice production.

5.2 SURFACE HEAT EXCHANGE

5.2.1 Radiation

All matter radiates energy in proportion to the fourth power of its absolute temperature

$$F^* = \varepsilon \sigma T_o^4 \qquad (5.1)$$

where F^* is the emitted radiation, ε = the emissivity of the material, σ = the Stefan-Boltzman constant = $8.13 \cdot 10^{-11}$ cal cm^{-2} min^{-1} $^oK^{-4}$ ($5.67 \cdot 10^{-8}$ W m^{-2} $^oK^{-4}$), and T_o = radiative temperature of the material. Most of the radiative energy reaching the surface of the Earth lies in two spectral bands: shortwave radiation which originates from the sun and has a maximum intensity near

a wavelength of 0.5 μ
from the earth and atmo
shown in Figure 1, th
derived from these two
tion in their measureme

Longwave radiatio
change in the polar
shortwave radiation (F
winter, and even at
only a few percent l
(F_L). The annual to
(Table 1). The magnit
tion of temperature an
increase in air temper
sponding increase in
magnitude of F_L, the n
heat from the ice.
the ice usually exceed
of radiation emitted
Net longwave losses a
fall due to the prese
amounts of water vapo
effective radiative t
of the surface. Fewe
large decrease in the
the effective temperat
atmosphere, causing a
surface.

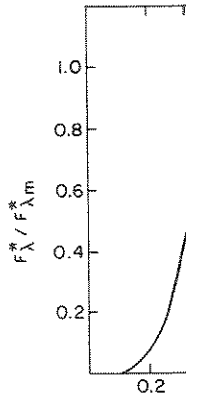

Fig. 1. Blackbody sp
to the sun (
at the wavel
and Businger

mass balance of ice-
to inaccessibility and
observations on the
ver, measurements have
I.S. and Soviet drifting
lucing substantial data
emperatures, snowfall,
ıy parts of the Arctic
ın, 1975). During the
ved across much of the
formation on the large
velocity, and surface
981; Thorndike et al.,
) been deployed in the
en generally limited to
the seasonal ice which
espite recent attention
seasonal ice, our gene-
he ice, the ocean, and
: has been seen in the
ic Basin. The applica-
ılly active areas such
ertain.

ill review the various
examine the relative
arctic ice pack. We
mass balance of a sea
redicting ice growth,
o changes in climate.
ın dynamic and thermo-
ıess variations affect
.

n to the fourth power

(5.1)

issivity of the mate-
.13 · 10^{-11} cal cm^{-2}
= radiative tempera-
e energy reaching the
ds: shortwave radia-
ıaximum intensity near

a wavelength of 0.5 μm, and longwave radiation which originates from the earth and atmosphere and has a maximum near 12 μm. As is shown in Figure 1, there is little overlap between the radiation derived from these two sources, giving rise to a natural separation in their measurement and treatment.

Longwave radiation. Longwave radiation dominates heat exchange in the polar regions during much of the year. Incoming shortwave radiation (F_r) is negligible during most of the fall and winter, and even at the height of the summer melt season F_r is only a few percent larger than the incoming longwave radiation (F_L). The annual total of F_L is more than double that of F_r (Table 1). The magnitude of F_L depends on the vertical distribution of temperature and water vapor in the atmosphere. The 30-40°C increase in air temperature from winter to summer produces a corresponding increase in F_L on the order of 80-90%. In spite of the magnitude of F_L, the net effect of longwave radiation is to remove heat from the ice. This is because the radiative temperature of the ice usually exceeds that of the atmosphere, so that the amount of radiation emitted by the ice ($F\uparrow$) almost always exceeds F_L. Net longwave losses are at a minimum during the summer and early fall due to the presence of extensive low clouds and substantial amounts of water vapor close to the surface. These result in an effective radiative temperature for the atmosphere close to that of the surface. Fewer and higher clouds during the winter and a large decrease in the amount of water vapor combine to increase the effective temperature differential between the ground and the atmosphere, causing an increase in the net longwave losses at the surface.

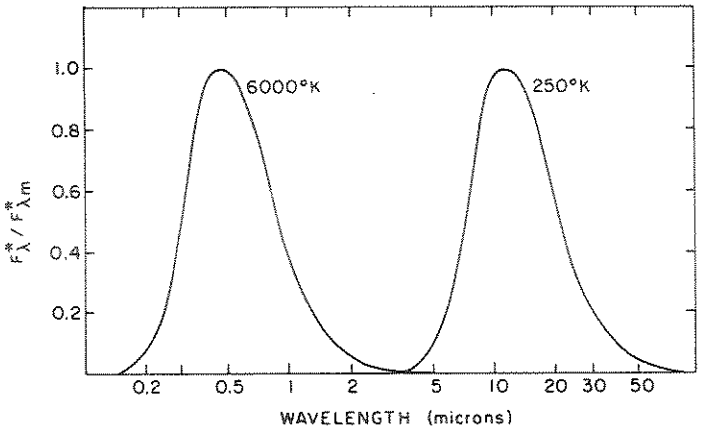

Fig. 1. Blackbody spectra for temperatures roughly corresponding to the sun (6000° K) and the earth (250° K), normalized at the wavelenth of maximum emission, λ_m. (After Fleagle and Businger, 1963).

Accurate measurements of F_L and $F\uparrow$ are particularly difficult in the polar regions where dew or frost formation on the transparent dome shielding the radiation sensor is a constant problem throughout the year. Because of the need for continual clearing and maintenance of the dome and problems with moisture inside the instrument, observations of longwave radiation are seldom carried out on a routine basis. However both F_L and F can be estimated from other information. Surface temperature data are frequently used with eq. (5.1) to calculate $F\uparrow$. Longwave emissivities (ε_L) of the ice, leads and melt ponds are all close to 0.97; $\varepsilon_L = 0.99$ when there is a snow cover.

If the vertical structure of temperature and humidity in the lower troposphere are known, F_L can be calculated by various techniques, e.g., Elsasser's method (Haltiner and Martin, 1957). Such data are generally not available in the polar regions, so these techniques are seldom used there. Because a large fraction of F_L is emitted by clouds and water vapor located relatively close to the ground, attempts to parameterize F_L on the basis of surface observations have been fairly successful. Air temperature (T_a) at screen height (2 m), the partial pressure of water vapor near the surface (e_a), and the fractional cloud cover (C) are all correlated with F_L, but the degree of correlation depends on geographic location. For example, a formula which produces good results in the tropics would not necessarily perform well in the polar regions. Longwave parameterizations have the form

$$F_L = \varepsilon^* \sigma T_a^4$$

where ε^* is an effective emissivity for the atmosphere and is a function of C and e_a. Three different formulations for ε^* have been developed for arctic conditions. Maykut and Church (1973) analyzed some 3000 sets of hourly observations of F_L, T_a, e_a, and C taken throughout an entire year at Barrow, Alaska and obtained the expression

$$\varepsilon^* = 0.7855(1 + 0.2232\, C^{2.75}) \quad . \tag{5.2}$$

Unlike studies at lower latitudes, they found no correlation between e_a and F_L, presumably because the average water vapor content ($\bar{e}_a$ = 1-2 mb) of the atmosphere is so low. With winds usually blowing from the ice pack, Barrow type conditions should obtain throughout much of the Arctic Basin. Equation (5.2) provided a fairly good match for the data -- the standard deviation of the percent difference between observed and predicted values was 12% under clear skies and 7% under overcast skies. The reason for the nonlinear dependence on cloudiness is uncertain, but a similar dependence has been reported by Laevastu (1960) for shortwave radiation and by Kirilova (1952) for longwave radiation.

Table 5.1. Radiation balance (MJ m^{-2} mo^{-1}) of perennial ice in the Central Arctic (Marshunova 1961; Maykut and Untersteiner 1971). Numbers in parentheses take into account the effects of summer melt ponds.

	Jan	Feb	Mar	Apr	May	Jun	Jul	Aug	Sep	Oct	Nov	Dec	Year
Incoming Longwave													

particularly difficult
ıation on the transpar-
is a constant problem
for continual clearing
th moisture inside the
.on are seldom carried
nd F can be estimated
'e data are frequently
wave emissivities (ε_L)
)se to 0.97; ε_L = 0.99

'e and humidity in the
:alculated by various
er and Martin, 1957).
he polar regions, so
:ause a large fraction
)r located relatively
ze F_L on the basis of
ful. Air temperature
essure of water vapor
oud cover (C) are all
ation depends on geo-
which produces good
y perform well in the
'e the form

atmosphere and is a
ulations for ε^* have
ut and Church (1973)
s of F_L, T_a, e_a, and
. Alaska and obtained

(5.2)

l no correlation be-
e water vapor content
With winds usually
itions should obtain
.on (5.2) provided a
ard deviation of the
cted values was 12%
The reason for the
ı, but a similar de-
for shortwave radia-
ion.

Table 5.1. Radiation balance (MJ m^{-2} mo^{-1}) of perennial ice in the Central Arctic (Marshunova 1961; Maykut and Untersteiner 1971). Numbers in parentheses take into account the effects of summer melt ponds.

	Jan	Feb	Mar	Apr	May	Jun	Jul	Aug	Sep	Oct	Nov	Dec	Year
Incoming Longwave Radiation [F_L]	435	430	430	495	630	750	800	780	690	580	475	450	6945
Outgoing Longwave Radiation [$F\uparrow$]	-520	-500	-505	-600	-725	-830	-835	-820	-720	-610	-535	-520	-7720
Net Longwave Radiation [$F_L + F\uparrow$]	-85	-70	-75	-105	-95	-80	-35	-40	-30	-30	-60	-70	-775
Incoming Shortwave Radiation [F_r]			100	420	730	785	575	370	155	20			3155
Absorbed Shortwave Radiation [$(1-\alpha)F_r$]			15	80	145	170	245 (295)	115 (165)	35	5			810 (910)
Net Radiation	-85	-70	-60	-25	50	90	210 (255)	75 (120)	5	-25	-60	-70	35 (125)

An alternate expression for ε^* in the Arctic, based on monthly averaged data, was suggested by Marshunova (1961)

$$\varepsilon^* = (0.67 + 0.05\sqrt{e_a})(1 + nC) \qquad (5.3)$$

where e_a is in mb and n is an empirical parameter which varies with season, being 0.22 in mid-summer and increasing to 0.30 in the winter. The linear dependence on cloudiness was justified because conditions in the Arctic are "usually either overcast or clear," so that conditions in between are not very important to the monthly averages. The effect of e_a in eq. (5.3) is to cause a 10-15% increase in ε^* between winter and summer, although this is partially compensated for by the decrease in n. The reason for such a dependence to show up in the monthly data and not in the hourly data of Maykut and Church is unknown.

Idso and Jackson (1969) derived a complex formula for ε^* under clear skies

$$\varepsilon_o^* = 1 - 0.261 \exp[-7.77 \cdot 10^{-4}(T_a - 273)^2] \quad . \qquad (5.4)$$

Using clear sky data from Barrow, we compared predictions made by eq. (5.4) with those of eq. (5.2) ($\varepsilon_o^* = 0.7855$) and found no discernible difference in the accuracy of the two methods. When eq. (5.4) was used in conjunction with Marshunova's (1+nC) cloud factor, the correlation between observed and predicted values was 0.78 as compared to the 0.92 obtained with eq. (5.2).

The dependence of F_L on T_a and C for the three expressions is shown in Figure 2. Equations (5.2) and (5.3) are fairly close for clear and overcast conditions, and both exhibit a stronger temperature dependence than eq. (5.4). Maximum differences in predicted values of F_L are 10-15%. Choice of the "best" parameterization is not really possible from this evidence. Equation (5.2) is supported by the most data, particularly when $0<C<1$, but was developed for use with short term averages; eq. (5.3) requires input on e_a and n(t), but appears to provide good long term averages; Idso and Jackson claim that eq. (5.4) fits their experimental data with a correlation coefficient of 0.992, but its application to the Barrow data leaves in doubt the value of the more complex expression. While the differences in F_L predictions seem small, they can lead to differences in the net longwave radiation totals of as much as 200-300%. Additional studies are needed to develop improved methods of estimating F_L -- particularly useful would be parameterizations using buoy and satellite observations.

Incoming Shortwave Radiation. Incoming shortwave radiation undergoes large seasonal variations in the polar regions, the sun being continuously above or below the horizon for 2-6 months at a

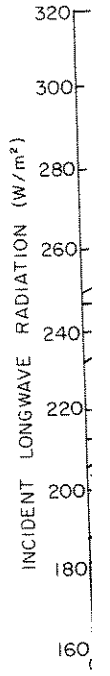

Fig. 2. Comparisor
ture (°C)
parameteri

time. Because of
ingly large. In
cover, monthly tot
1) equal or excee
such as New York
there is little s
Arctic Basin durin
ation reaching the
due to the extreme
Table 1 clearly
solstice -- much
May and early Ju
results from (i)
throughout the su
radiation caused h

At low and m
commonly reduce F
of their thinnes

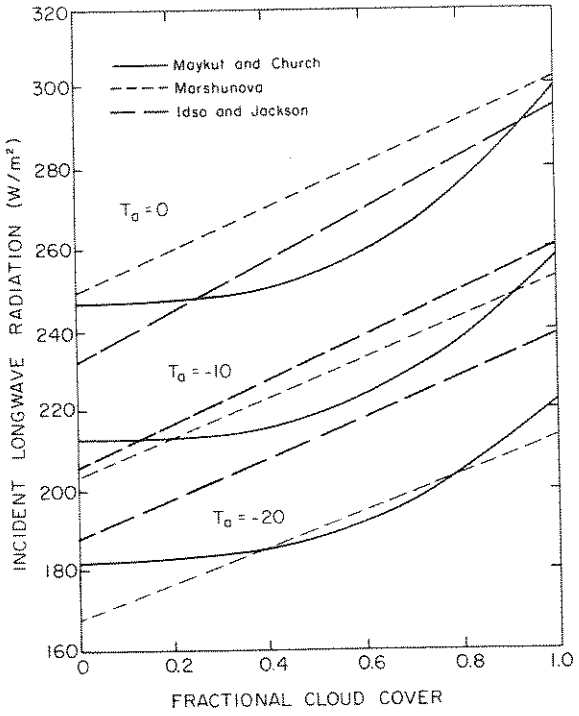

Fig. 2. Comparison of the effects of cloudiness and air temperature (°C) on incoming longwave radiation as predicted by parameterizations developed for polar conditions.

time. Because of the long days, summer values of F_r are surprisingly large. In spite of the low sun angle and extensive cloud cover, monthly totals for May and June in the Central Arctic (Table 1) equal or exceed those measured at many mid-latitude stations such as New York and Chicago. According to Marshunova (1961), there is little spatial variation in monthly F_r totals across the Arctic Basin during the summer months. Most of the shortwave radiation reaching the surface of the ice is diffuse rather than direct due to the extreme cloudiness ($\bar{C}>0.9$ from June through September). Table 1 clearly shows that F_r is asymmetric about the summer solstice -- much more shortwave energy arrives at the surface in May and early June than in late June and July. This skewness results from (i) increasing optical thickness of the atmosphere throughout the summer warming, and (ii) a decrease in the diffuse radiation caused by decreasing surface albedo.

At low and mid-latitudes, reflection and absorption by clouds commonly reduce F_r at the surface by as much as 80-90%. Because of their thinness and low water content, arctic clouds rarely

decrease the incoming shortwave radiation by more than 50% (Vowinckel and Orvig, 1962). Under clear skies only about 45% of F_r lies in the visible region (0.4-0.7 μm); under overcast skies this figure increases to about 65%. Light absorption by clouds in the near-infrared (0.7-2.5 μm) increases with increasing wavelength. Optical measurements (Grenfell and Perovich, 1984) indicate that arctic clouds absorb nearly all the energy above 1.4 μm, but transmit substantial amounts in the 0.7-1.4 μm region (Fig. 3). Attenuation at 1.2 μm is roughly three times as large as at 0.7 μm. An example of how seasonal variations in cloud cover affect the transmission of light through the entire thickness of the atmosphere in the polar regions is given in Figure 4. As is to be expected, the total transmissivity (τ) is sensitive to atmospheric moisture content -- maximum values occur in the spring when T_a and e_a are still low, but solar elevation high. The general trend toward smaller values of τ in all cloud categories after April reflects increasing moisture content of the air and thicker clouds.

Although shortwave measurements are less troublesome than longwave ones, parameterizations of F_r are frequently useful in large-scale heat balance studies and numerical modeling (e.g., Parkinson and Washington, 1979). Parameterizations of F_r generally

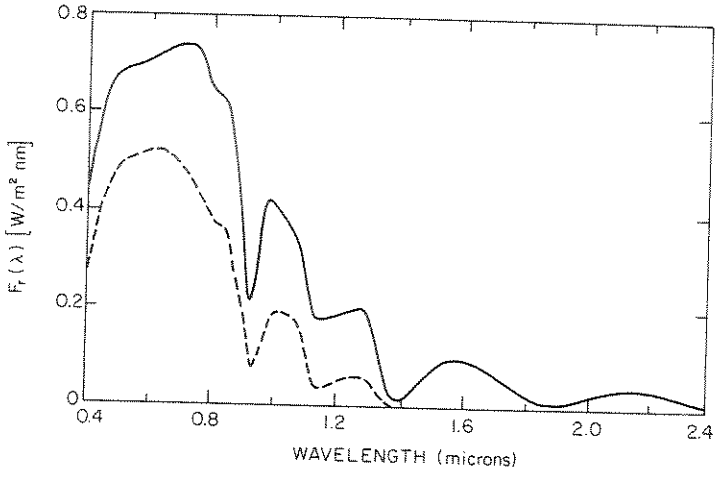

Fig. 3. The effect of a heavy overcast on the spectral distribution of incident shortwave radiation during the early summer at Point Barrow, Alaska. The decrease in the total amount of incident shortwave radiation from clear sky conditions (solid curve) to overcast conditions (dashed curve) is about 45%. (After Grenfell and Perovich, 1984).

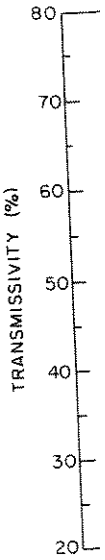

Fig. 4. The relat
cover and
and Churc

have the form

$$F_r = a^* F_o$$

where F_o is the
the absence of cl
tion by clouds.
and F_r can be
transfer models
1975), but the pr
routine applicati
empirical relatic
radiation depleti
ient form for F_o

$$F_o = \frac{\quad}{1.085\ c}$$

where S_o is the
zenith angle, a

To judge th
first at daily

n by more than 50%
:ies only about 45% of
; under overcast skies
)sorption by clouds in
with increasing wave-
Perovich, 1984) indi-
e energy above 1.4 μm,
.4 μm region (Fig. 3).
as large as at 0.7 μm.
loud cover affect the
:ickness of the atmos-
ure 4. As is to be
nsitive to atmospheric
he spring when T_a and
. The general trend
ories after April re-
and thicker clouds.

ess troublesome than
frequently useful in
ical modeling (e.g.,
tions of F_r generally

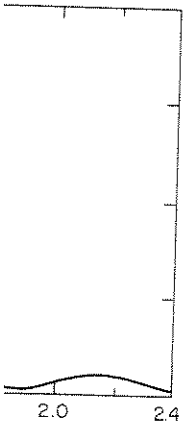

e spectral distribu-
n during the early
he decrease in the
adiation from clear
overcast conditions
After Grenfell and

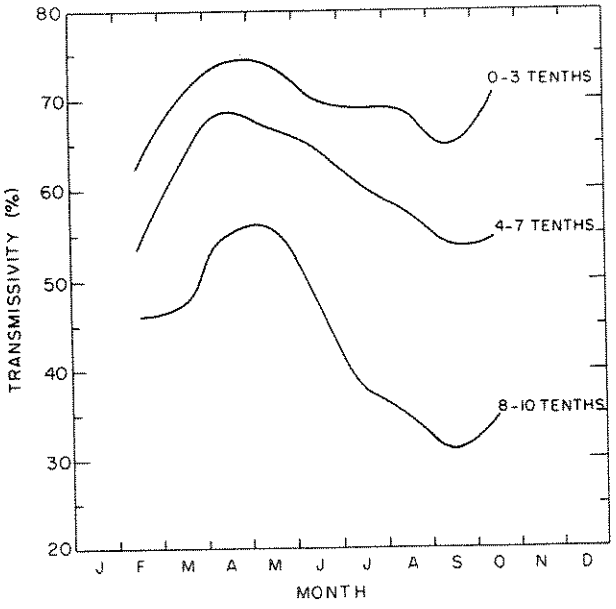

Fig. 4. The relation of total atmospheric transmissivity to cloud cover and season at Point Barrow, Alaska. (After Maykut and Church, 1973).

have the form

$$F_r = a^* F_o$$

where F_o is the downwelling shortwave radiation at the surface in the absence of clouds, and a^* represents the fractional attenuation by clouds. F_o depends on hour, day and latitude. Both F_o and F_r can be calculated theoretically from various radiative transfer models of the atmosphere (e.g., Leckner, 1978; Wiscombe, 1975), but the procedures are generally too involved to be used in routine applications. Cruder estimates of F_o can be obtained from empirical relationships between air mass, water vapor content, and radiation depletion (e.g., Houghton, 1954). A particularly convenient form for F_o was given by Zillman (1972)

$$F_o = \frac{S_o \cos^2 Z}{1.085 \cos Z + (2.7 + \cos Z) e_a \cdot 10^{-3} + 0.1} \qquad (5.5)$$

where S_o is the solar constant, e_a is in mb, and Z is the solar zenith angle, a function of latitude, day, and hour.

To judge the performance of eq. (5.5) in the Arctic, we looked first at daily totals of F_r from Point Barrow under clear skies

and calculated the ratio (R) of the predicted F_o to the observed F_o (see Table 2). Equation (5.5) underestimated daily totals throughout the spring, but the error decreased as temperatures warmed until late in the melt season when eq. (5.5) began to overestimate F_o. Monthly values of F_o have been tabulated throughout the Arctic Basin by Vowinckel and Orvig (1962b). Comparison of monthly totals derived from integrating eq. (5.5) with those given by Vowinckel and Orvig at various latitudes between 70 and 90°N indicates that eq. (5.5) consistently underestimates F_o - by an average of 14% in May, 7% in June, 3% in July, and 6% in August. The reason is probably related to the smaller amount of water vapor in the polar atmosphere and to multiple scattering of reflected radiation between the ice and clouds. All in all, the Zillman equation performs quite well, but it appears that a high latitude correction may be desirable over the pack ice. On the basis of model calculations, Shine (1984) reports that improved performance can be obtained from eq. (5.5) over ice and snow if the denominator is changed to $\cos Z + (1 + \cos Z)\, e_a \cdot 10^{-3} + 0.046$.

A summary of Soviet investigations into the effect of cloudiness on F_r in the Arctic has been given by Marshunova (1961). They were able to obtain good agreement with observations with an expression of the form

$$a^* = 1 - kC \qquad (5.6)$$

where k depends on season (i.e., cloud thickness), increasing from 0.15 in March to 0.5 in July and August. When compared with daily values of C and F_r observed at Point Barrow, eqs. (5.5) and (5.6) generally produced agreement to within 10-15%. Equation (5.6), however, provided no consistent agreement between monthly values when used with the data of Vowinckel and Orvig (1962b, 1962c). Laevastu (1960) suggested that

$$a^* = 1 - 0.6C^3 \quad . \qquad (5.7)$$

When tested with the Point Barrow data under overcast conditions, eq. (5.7) always underestimated F_r, in some cases by as much as 40-50%. Equation (5.7) thus appears to be more suitable for describing the effects of lower latitude clouds. Surprisingly, when used with the monthly data of Vowinckel and Orvig, eq. (5.7)

Table 5.2. Ratio of predicted F_o to observed F_r for clear days at Point Barrow.

Date	1 March	22 March	7 April	30 May	12 August
R	0.76	0.80	0.92	0.95	1.08

produced monthly totals
ally agreed with their
close agreement is u
quite limited (0.75-0.9

Optical Propertie
of the ice determine
We shall be concerned
extinction coefficient
reflected to incident
when the ice is covere
blown snow, albedos ar
snow warms and becomes
0.70-0.75 at the onset
quite variable, depen
surface. Measurements
0.70 and 0.75 when the
the ice is melting;
0.5-0.6 when it is co
albedos of multiyear
and a thicker scatter
meltwater puddles du
amount of shortwave
albedos vary over a
in the melt season to

Spectral albedos
Maykut (1977) over mar
shows albedos of sev
Albedos are fairly c
nm) spectrum, but be
lengths. There is lit
and melting multiyear
liquid water content
the infrared produci
There are two main s
water saturated blue
drained, granular sur
the blue ice. Spect
close to those of th
but are much smaller
is that light penetr
determined by the pro
lengths, backscatter
comes important. I
there is less backsca
600 nm range, hence
decrease in the albe
lengths is due to t
wavelengths to increa

produced monthly totals of F_r between May and September which usually agreed with their values to within 10%. The reason for such close agreement is uncertain, but the range in cloudiness was quite limited (0.75-0.90).

Optical Properties of the Ice Pack. The optical properties of the ice determine how it interacts with shortwave radiation. We shall be concerned here primarily with the albedo (α) and the extinction coefficient (κ). The albedo is defined as the ratio of reflected to incident shortwave radiation. During the winter, when the ice is covered by fairly dense ($\bar{\rho}_s$ = 0.35 Mg m^{-3}) wind blown snow, albedos are typically in the range 0.80-0.85. As the snow warms and becomes more dense, its albedo decreases to about 0.70-0.75 at the onset of melting. The albedo of bare sea ice is quite variable, depending on temperature, age, and state of the surface. Measurements on thick perennial ice give albedos between 0.70 and 0.75 when the ice is cold, and between 0.55 and 0.70 when the ice is melting; albedos of thick (1-2 m) first-year ice are 0.5-0.6 when it is cold and 0.3-0.5 during melting. The larger albedos of multiyear ice are due to a higher vapor bubble density and a thicker scattering layer at the surface. The presence of meltwater puddles during the summer melt season increase the amount of shortwave radiation absorbed by the ice pack. Pond albedos vary over a wide range, from 0.4 for shallow ponds early in the melt season to 0.15 for deep ones at the end of the summer.

Spectral albedos (α_λ) have been measured by Grenfell and Maykut (1977) over many types of surfaces in the Arctic. Figure 5 shows albedos of several kinds of first-year and multiyear ice. Albedos are fairly constant across most of the visible (400-700 nm) spectrum, but begin to decrease upon reaching the red wave lengths. There is little difference between the albedos of frozen and melting multiyear ice in the visible region, but the increased liquid water content of the melting ice increases absorption in the infrared producing a substantial decrease in $\alpha(\lambda > 700$ nm). There are two main surface types on melting first-year ice: (i) water saturated blue ice and (ii) white ice which consists of a drained, granular surface layer 5-10 cm in thickness underlain by the blue ice. Spectral albedos of first-year white ice are very close to those of the melting multiyear ice at long wavelengths, but are much smaller at shorter wavelengths. The reason for this is that light penetration is small at long wavelengths so α_λ is determined by the properties of the surface layer; at shorter wavelengths, backscatter from the ice beneath the surface layer becomes important. In the case of melting first-year white ice, there is less backscatter from the underlying blue ice in the 400-600 nm range, hence the observed decrease in α_λ. The further decrease in the albedo of the blue ice (curve d) at short wavelengths is due to the absence of the white layer, and at longer wavelengths to increased liquid water in the surface layer.

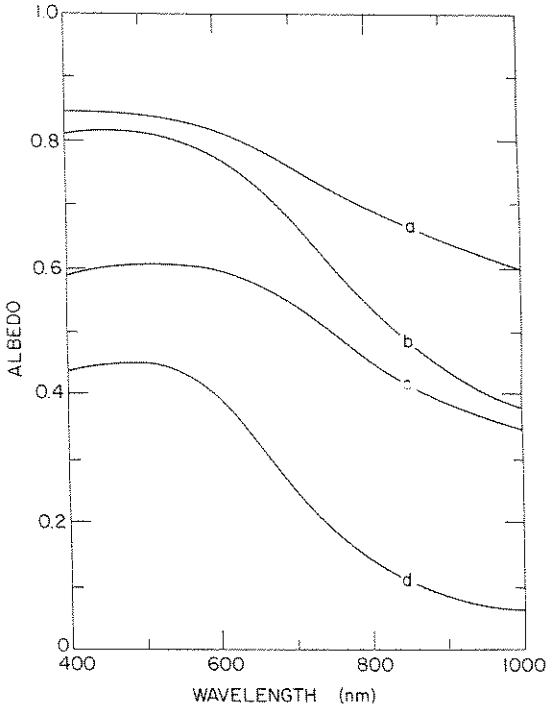

Fig. 5. Spectral albedos observed over bare sea ice: (a) frozen multiyear ice, (b) melting multiyear ice, (c) melting first-year white ice, and (d) melting first-year blue ice (after Grenfell and Maykut, 1977).

Figure 6 shows spectral albedos observed over snow and melt ponds. The albedo of dry compact snow is high and has only a weak dependence on λ. Increasing density and liquid water content decrease α_λ, particularly in the infrared. The albedos of both snow and ice decrease strongly above 1000 nm, reaching values of 0.1 or less at 1400 nm (Grenfell and Perovich, 1984). The albedo of pond covered ice is characterized by a maximum at short wavelengths and a dramatic decrease between 500 and 800 nm. Because water in the ponds is relatively transparent at short wavelengths, values below 500 nm are determined primarily by the scattering properties of the underlying ice. The transition zone (500-800 nm) represents a region where α_λ becomes increasingly insensitive to the underlying ice as absorption by the water becomes the dominant factor. Above 800 nm absorption by the water is so large that α_λ is determined only by Fresnel reflection from the pond surface. Thus most of the albedo difference between individual ponds occurs in the visible where it is readily apparent to the naked eye.

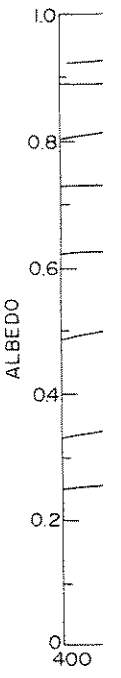

Fig. 6. Spectral albed
snow, (b) wet
melt pond with
(f) mature mel
(h) old melt p

The total albedo

$$\alpha = \frac{\int \alpha_\lambda F_r(\lambda) d\lambda}{\int F_r(\lambda) d\lambda}$$

Although α_λ is indepe
the total albedo, the
α_λ and the spectral d
is because clouds remo
long wavelengths than
from the more reflect
more heavily in the
of summer albedos unde
Table 3.

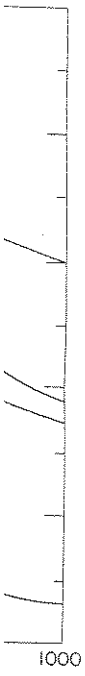

ea ice: (a) frozen
ice, (c) melting
first-year blue ice

over snow and melt
nd has only a weak
l water content de-
bedos of both snow
ng values of 0.1 or
The albedo of pond
ort wavelengths and
cause water in the
ngths, values below
ring properties of
00 nm) represents a
to the underlying
iant factor. Above
α_λ is determined
ce. Thus most of
ls occurs in the
l eye.

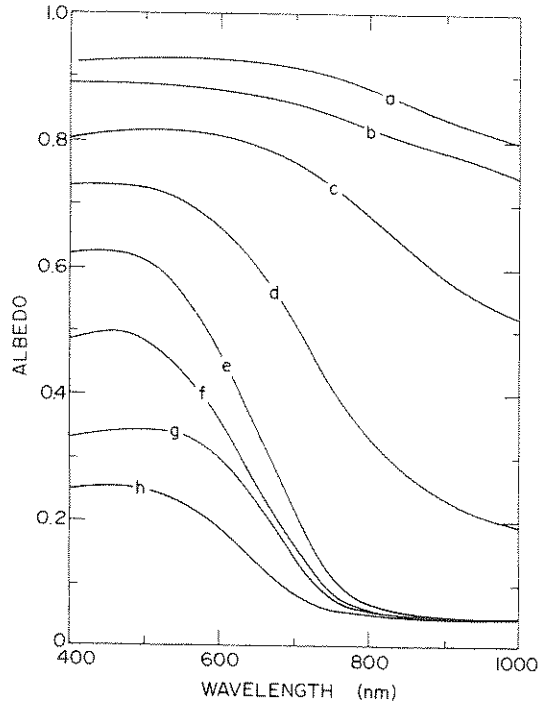

Fig. 6. Spectral albedos observed over snow and melt ponds: (a) dry snow, (b) wet new snow, (c) melting old snow, (d) frozen melt pond with 3 cm of ice, (e) early season melt pond, (f) mature melt pond, (g) melt pond on first-year ice, and (h) old melt pond (after Grenfell and Maykut, 1977).

The total albedo can be expressed as

$$\alpha = \frac{\int \alpha_\lambda F_r(\lambda) d\lambda}{\int F_r(\lambda) d\lambda} .$$

Although α_λ is independent of cloudiness, clouds tend to increase the total albedo, the size of the increase being dependent on both α_λ and the spectral distribution of the incident radiation. This is because clouds remove proportionately more energy from $F_r(\lambda)$ at long wavelengths than short ones (Figure 3), so that contributions from the more reflective shorter wavelength region are weighted more heavily in the integral when the sky is overcast. Examples of summer albedos under clear and overcast skies are presented in Table 3.

Table 5.3. Total albedo as a function of ice type and cloud cover during the summer melt season. (After Grenfell and Maykut, 1977).

Ice Type	Clear	Overcast
Old snow	0.63	0.77
White ice	0.56	0.70
First year blue ice	0.25	0.32
Mature melt pond	0.22	0.29

Scattering and absorption cause light to be attenuated as it passes through the ice. This attenuation is characterized by a spectral extinction coefficient

$$\kappa_\lambda = \frac{1}{-F(z,\lambda)} \frac{dF}{dz} \tag{5.8}$$

where $F(z,\lambda)$ is the downward shortwave flux at a depth z and wavelength λ. Figure 7 shows measured values of κ_λ for various types of ice and snow. Extinction coefficients in all cases were relatively constant in the 400-500 nm region, but increased sharply at longer wavelengths--κ_λ at 750 nm was typically 4-5 times as large as at 500 nm. The greatest attenuation was observed in cold snow where κ_λ's were roughly 4 times as large as those in the surface layer and about 20 times those of the interior ice. With the onset of melting, κ_λ's in the snow decreased by a factor of 2. The transition zone in Figure 7 describes a 10-15 cm thick region where the decomposed surface layer grades into the more uniform interior ice. The difference between κ_λ's for first-year and multiyear interior ice were caused by differences in brine volume and bubble density. The low values observed in curve (f) were the result of extremely large brine volumes (20-55%) in the ice beneath the pond.

Experimental evidence (Grenfell and Maykut, 1977) indicates that κ_λ is independent of depth as long as the ice is reasonably uniform. The flux at any depth within this homogeneous layer can be found by integrating eq. (5.8) to obtain Beer's law

$$F(z,\lambda) = F(0,\lambda)e^{-\kappa_\lambda z} \tag{8}$$

where $F(0,\lambda)$ is the net shortwave radiation at the surface at wavelength λ. For practical applications, however, it is usually the total flux in the ice, $F_z = \int_0^\infty F(z,\lambda)d\lambda$, which is of interest. If we define the bulk extinction coefficient as the ratio of the total energy absorbed at depth z to the total flux at depth z, then

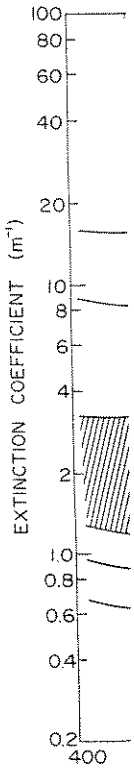

Fig. 7. Spectral exti
and snow: (
surface layer
multiyear ice
ice beneath
1977).

$$-\kappa_z = \frac{\int \kappa_\lambda F(0,\lambda)e^{-}}{\int F(0,\lambda)e^{-}}$$

and it follows from Be

$$F_z = F_o\, e^{-\int \kappa_z dz}$$

where F_o is the net
$\int_0^\infty (1-\alpha)\, F(0,\lambda)d\lambda$. G
both first-year and

ype and cloud cover
After Grenfell and

Overcast
0.77
0.70
0.32
0.29

be attenuated as it
characterized by a

(5.8)

depth z and wave-
for various types
ll cases were rela-
ncreased sharply at
4-5 times as large
served in cold snow
ose in the surface
ce. With the onset
or of 2. The tran-
thick region where
re uniform interior
-year and multiyear
volume and bubble
were the result of
e beneath the pond.

it, 1977) indicates
ice is reasonably
mogeneous layer can
's law

(8)

at the surface at
ever, it is usually

ch is of interest.

is the ratio of the
flux at depth z,

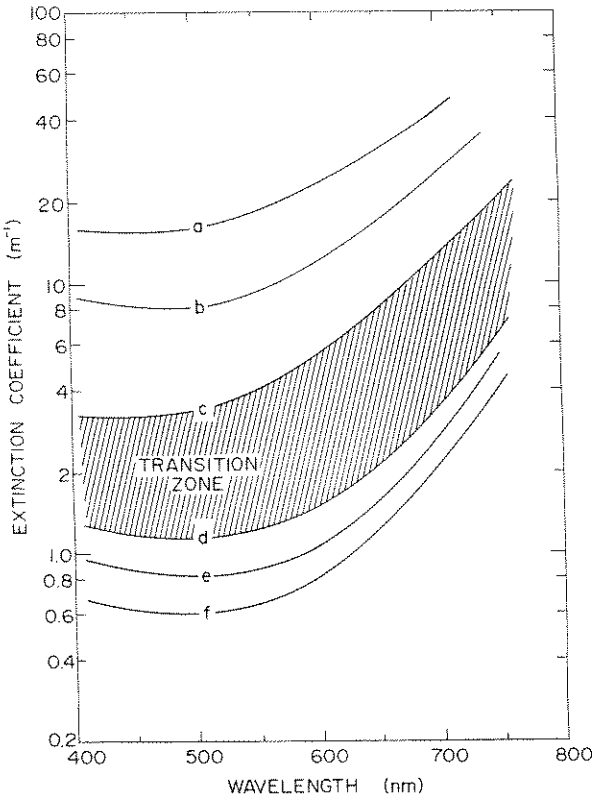

Fig. 7. Spectral extinction coefficients for various types of ice and snow: (a) dry compact snow, (b) melting snow, (c) surface layer on melting multiyear ice, (d) interior of multiyear ice, (e) interior of first-year ice, and (f) ice beneath an old melt pond (after Grenfell and Maykut, 1977).

$$-\kappa_z = \frac{\int \kappa_\lambda F(0,\lambda) e^{-\kappa_\lambda z} d\lambda}{\int F(0,\lambda) e^{-\kappa_\lambda z} d\lambda} ,$$

and it follows from Beer's law that

$$F_z = F_o \, e^{-\int \kappa_z dz} \qquad (5.9)$$

where F_o is the net total shortwave radiation at the surface, $\int_0^\infty (1-\alpha) F(0,\lambda) d\lambda$. Grenfell and Maykut have calculated κ_z's for both first-year and multiyear ice (Figure 8). They found that

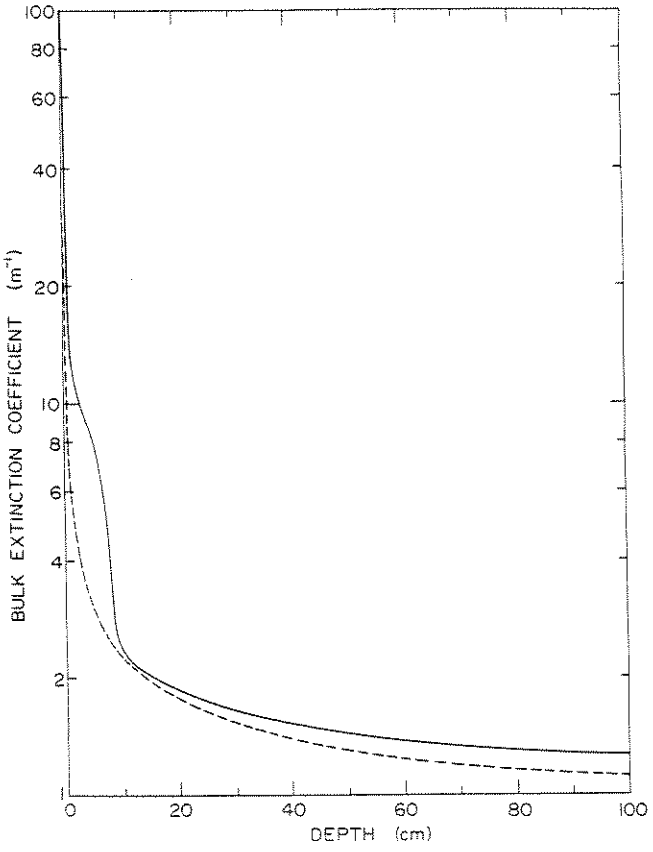

Fig. 8. Bulk extinction coefficients in multiyear ice (solid curve) and first-year blue ice (dashed curve). (After Grenfell and Maykut, 1977).

κ_z's depend strongly on z in the upper 10-20 cm, but have only a weak dependence below this. Bulk extinction coefficients below 5 cm were not affected by cloudiness. Bulk values in the lower part of the ice were in good agreement with Untersteiner (1961) and Chernigovskii (1963) who measured average extinction coefficients of 1.5 m^{-1} in perennial ice.

Absorbed and Penetrating Shortwave Radiation. The net input of shortwave radiation at the surface of the ice is simply $(1-\alpha)F_r$. Monthly averages over perennial arctic ice are shown in Table 1. About 85% of the annual total is absorbed between the first of May and the end of August. Although F_r is largest in June, the high albedo of the snow cover reduces the June total below that of July. Complicating shortwave absorption in the summer Arctic are low albedo melt ponds whose areal coverage varies greatly in both time

and space. Coverage during the final stages about 30% once the ice tion reduce the areal e producing values of ab relief, initial melting complete pond coverage account for 60% or mo ice. This pattern do appear to be uncommon. tht ponds are not a balance of the Antarcti

A rough estimate c sorption in the Centra an average pond covera According to Langleben albedos of 0.49 in Ju input to the ice pack the year. Pond effects ice where average albe areas, melting is enha presence of wind-borne play an important role al arctic ice, their i limited. In the latte is stored as latent he eventually released to Theoretical calculation that this temporary he thickness of perennial

Because ice is a wave radiation (I_o) is does not immediately c the surface. Accurat requires some method o ments made in multiyea (Untersteiner, 1961) i radiation is stored as being used directly (Grenfell and Maykut, to the amount of ene white ice. Thus, it a = 10 cm). If we defin radiation transmitted b

$$I_o = i_o(1 - \alpha)F_r$$

Grenfell and Maykut s

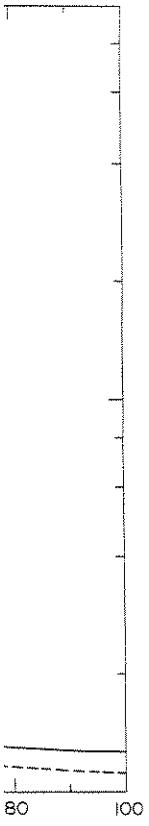

ıultiyear ice (solid
ıhed curve). (After

cm, but have only a
coefficients below 5
ıes in the lower part
:ersteiner (1961) and
tinction coefficients

ıtion. The net input
.ce is simply $(1-\alpha)F_r$.
ıre shown in Table 1.
ween the first of May
:st in June, the high
ıl below that of July.
ımmer Arctic are low
greatly in both time

and space. Coverage on multiyear ice may briefly reach 50-60% during the final stages of snow melt, but it quickly decreases to about 30% once the ice becomes snow-free. Deepening and consolidation reduce the areal extent of these ponds throughout the summer, producing values of about 10% by late August. Due to low surface relief, initial melting on first-year ice often results in nearly complete pond coverage. Even late in the melt cycle, ponds can account for 60% or more of the surface area on seasonal arctic ice. This pattern does not occur in the Antarctic where ponds appear to be uncommon. For this reason it is generally believed tht ponds are not a significant factor in the heat and mass balance of the Antarctic ice pack.

A rough estimate of the effects of melt ponds on shortwave absorption in the Central Arctic is presented in Table 1, assuming an average pond coverage of 30% during July and 10% during August. According to Langleben (1971), this would result in area averaged albedos of 0.49 in July and 0.56 in August, increasing shortwave input to the ice pack by 20% in July, 40% in August, and 12% for the year. Pond effects are somewhat greater in regions of seasonal ice where average albedos may drop as low as 35-40%. In coastal areas, melting is enhanced not only by the ponds, but also by the presence of wind-borne dust from the nearby land. While ponds play an important role in the decay, breakup and retreat of seasonal arctic ice, their impact on multiyear ice appears to be more limited. In the latter case much of the absorbed shortwave energy is stored as latent heat in ponds and brine pockets where it is eventually released to the atmosphere during the fall freeze-up. Theoretical calculations (Maykut and Untersteiner, 1971) indicate that this temporary heat storage has little effect on the average thickness of perennial ice.

Because ice is a translucent material, part of the net shortwave radiation (I_o) is transmitted through the surface layer and does not immediately contribute to temperature or mass changes at the surface. Accurate prediction of surface changes therefore requires some method of estimating the magnitude of I_o. Measurements made in multiyear white ice during the summer melt season (Untersteiner, 1961) indicate that about 30% of the net shortwave radiation is stored as latent heat within the ice, rather than being used directly at the surface. Theoretical calculations (Grenfell and Maykut, 1977) show that this is roughly equivalent to the amount of energy transmitted through the upper 10 cm of white ice. Thus, it appears reasonable to assume that $I_o \approx F_z$ (z = 10 cm). If we define i_o to be the fraction of the net shortwave radiation transmitted below 10 cm, then

$$I_o = i_o(1 - \alpha)F_r \quad . \tag{5.10}$$

Grenfell and Maykut show that i_o depends on α_λ, κ_λ, and the

spectral distribution of the incident radiation, then calculate the effects of cloudiness on i_o for various types of melting sea ice (Table 4). The fact that κ_z does not depend strongly on ice type, cloudiness, or depth in the interior of the ice suggests a simple way to estimate F_z below 10 cm. From eqs. (5.9) and (5.10) it follows that

$$F_z = i_o(1 - \alpha)F_r e^{-\bar{\kappa}(z - 0.1)} \tag{5.11}$$

where $\bar{\kappa}$ is the average bulk extinction coefficient in the lower part of the ice. Equation 5.11 provides the best fit to observations when $\bar{\kappa} = 1.5\ m^{-1}$

5.2.2 Turbulent Heat Exchange

Sensible heat is transferred across the lower part of the boundary layer as a result of temperature differences between the ice and atmosphere. Energy is likewise exchanged by the release of latent heat associated with evaporation, condensation, and sublimation. Apart from emitted longwave radiation, the sensible (F_s) and latent (F_e) heat fluxes are the only means of transporting energy from the surface into the atmosphere. Discussions of the surface energy balance in polar regions frequently dismiss F_s and F_e as being one to two orders of magnitude smaller than the radiation fluxes. However, while the individual radiation components are indeed large, the net radiation balance is small (Table 1) and contributions made by F_s and F_e become significant when compared with the net radiation. Theoretical calculations (Maykut and Untersteiner, 1969) have, for example, shown that the thickness of multiyear arctic ice is very sensitive to changes in F_s and F_e during the summer, indicating that the turbulent fluxes are an integral part of both the heat and the mass balance of an ice cover.

The rate at which heat is transferred by the turbulent fluxes depends on the roughness of the surface, the speed of the wind, the stability of the boundary layer, and the size of the temperature and water vapor gradients. Unfortunately the turbulent fluxes do not lend themselves readily to direct measurements. Eddy

Table 5.4. Fraction of the net shortwave radiation reaching a depth of 10 cm (i_o) in melting sea ice according to Grenfell and Maykut (1977).

Ice Type	Clear	Overcast
White ice	.18	.35
Blue ice/melt ponds	.43	.63

correlation methods ar
been applied for only
of F_s and F_e have be
various assumptions ab
commonly used paramete

$$F_s = \rho c_p C_s u(T_a - T$$

and

$$F_e = \rho L C_e u(q_a - q_c$$

where ρ is the density
air, T_a is the air te
10 m), T_o is the tempe
at the reference heigh
and q_a are specific hum
and C_s and C_e are bu
latent heat (Deardorff,
in terms of the partia
total atmospheric press

$$q = \frac{0.622e}{P - 0.378e} \simeq \frac{0}$$

since $P >> e$. Air at t
rated so that eq. (5.13

$$F_e = 0.622\rho L C_e u(re$$

where r is the relative
the saturation vapor pr
expressions have been o
Clausius-Clapeyron equa
Richards, 1971; Maykut,

Turbulent heat fl
over multiyear arctic s
mates of Badgley (1966
at U.S. Drifting Stat
(1963) were obtained
tions. The most compr
et al. (1978) who repo
the year using observat
Joint Experiment (AIDJ
situation over tempera
during much of the p
Even during the summer
change. In July and A
tudes of F_s and F_e are

correlation methods are difficult under arctic conditions and have been applied for only short periods of time. Most determinations of F_s and F_e have been derived by profile methods which contain various assumptions about the structure of turbulence. The most commonly used parameterizations are

$$F_s = \rho c_p C_s u(T_a - T_o) \tag{5.12}$$

and

$$F_e = \rho L C_e u(q_a - q_o) \tag{5.13}$$

where ρ is the density of the air, c_p is the specific heat of the air, T_a is the air temperature at some reference height (usually 10 m), T_o is the temperature of the surface, u is the wind speed at the reference height, L is the latent heat of vaporization, q_o and q_a are specific humidities at the surface and reference level, and C_s and C_e are bulk transfer coefficients for sensible and latent heat (Deardorff, 1968). Specific humidity can be expressed in terms of the partial pressure (mb) of water vapor (e) and the total atmospheric pressure (P)

$$q = \frac{0.622e}{P - 0.378e} \simeq \frac{0.622e}{P}$$

since $P >> e$. Air at the surface of the ice is assumed to be saturated so that eq. (5.13) is frequently written

$$F_e = 0.622\rho L C_e u(re_{sa} - e_{so})/P \tag{5.14}$$

where r is the relative humidity at the reference level and e_s is the saturation vapor pressure, a function of temperature. Numerous expressions have been obtained for $e_s(T)$ either by integrating the Clausius-Clapeyron equation or by fitting empirical data (e.g., Richards, 1971; Maykut, 1977).

Turbulent heat flux values obtained by profile techniques over multiyear arctic sea ice are compared in Table 5. The estimates of Badgley (1966) were based on half-hourly averages taken at U.S. Drifting Station Alpha, while the results of Doronin (1963) were obtained from data gathered at several Soviet stations. The most comprehensive calculations are those of Leavitt et al. (1978) who reported 6 hour totals of F_s and F_e throughout the year using observations taken during the Arctic Ice Dynamics Joint Experiment (AIDJEX). These results show that, unlike the situation over temperate and tropical oceans, F_e is negligible during much of the polar year (November-April in the Arctic). Even during the summer, F_e fails to dominate the turbulent exchange. In July and August, for example, the average daily magnitudes of F_s and F_e are nearly equal. Values given by Doronin for

Overcast
.35
.63

Table 5.5. Comparison of turbulent heat fluxes (MJ/m^{-2} mo^{-1}) observed over perennial ice in the Central Arctic.

		Jan	Feb	Mar	Apr	May	Jun	Jul	Aug	Sep	Oct	Nov	Dec	Year
F_s	Doronin	49	32	30	12	-19	-12	-13	-17	-7	4	23	33	115
	Badgley	29	23	25	0	-23	-28	0	-7	-13	4	11	16	37
	Leavitt et al.	15	13	11	15	7	-5	2	0	0	5	10	13	86
F_e	Doronin	0	-1	-1	-4	-19	-29	-27	-28	-16	-8	0	0	-133
	Badgley	0	0	0	0	-18	-23	-13	-2	9	11	7	2	-27
	Leavitt et al.	1	0	-2	-1	-9	-6	-7	-8	-14	-8	-1	-1	-56

both F_s and F_e tend
Leavitt et al. Doroni
times as large as th
shows substantial heat
et al. find relative
Badgley's results are
Leavitt et al. took
the smaller winter v
realistic description
boundary layer. The
ever, obscure the v
season. Daily totals
F_s has about the sam
winter. The differe
negative values alte
totals. Surprisingly
what higher during the

It is not clear
values for F_s and F_e
in measurement or ana
certainity in the pr
transfer coefficients.
al. (1973) yielded av
$\cdot 10^{-3}$. Observatio
refreezing lead (Lind
close to $3 \cdot 10^{-3}$ for
measurements carried
relatively uniform mu
of an order of magnit
es in surface geometry
the drag coefficient
1980). At this point
and temporal variatio
constitutes represent
the ice pack. Low le
spatial changes, but
are needed to monitor

While a few meas
coastal sites in the
tude elsewhere in the
indicates that turbul
than in the Arctic an
spondingly more impor
Antarctic sea ice. A
ice in the two hemis
that lower relative h
the Antarctic lead to
large to inhibit sur

both F_s and F_e tend to be larger than those of either Badgley or Leavitt et al. Doronin's winter totals of F_s are consistently 2-3 times as large as those of Leavitt et al.; in the summer Doronin shows substantial heat losses due to both F_s and F_e, while Leavitt et al. find relatively small losses due almost entirely to F_e. Badgley's results are intermediate between those of the other two. Leavitt et al. took into account the effects of stability, hence the smaller winter values for F_s could be the result of a more realistic description of conditions in the highly stable winter boundary layer. The small summer totals of Leavitt et al., however, obscure the vigor of turbulent transfer during the melt season. Daily totals obtained from Leavitt et al. indicate that F_s has about the same magnitude during the summer as during the winter. The difference is that during the summer positive and negative values alternate frequently, resulting in small monthly totals. Surprisingly, the variance of the daily totals is somewhat higher during the summer than during the winter.

It is not clear what portion of the differences in reported values for F_s and F_e are real and what portion are due to errors in measurement or analysis techniques. Probably the greatest uncertainity in the profile method is in the choice of suitable transfer coefficients. Eddy correlation measurements by Thorpe et al. (1973) yielded average values of $C_s = 1.2 \cdot 10^{-3}$ and $C_e = 0.55 \cdot 10^{-3}$. Observations in the unstable boundary layer over a refreezing lead (Lindsay, 1976; Andreas, 1980) gave average values close to $3 \cdot 10^{-3}$ for both C_s and C_e. However, roughness length measurements carried out by Untersteiner and Badgley (1965) on relatively uniform multiyear sea ice suggest temporal variations of an order of magnitude in the transfer coefficients. Differences in surface geometry (hummocks, pressure ridges, etc.) can change the drag coefficient by as much as a factor of two (Banke et al., 1980). At this point we lack sufficient information about spatial and temporal variations to say with any degree of confidence what constitutes representative values for the turbulent fluxes over the ice pack. Low level aircraft measurements can provide data on spatial changes, but ground-based eddy correlation measurements are needed to monitor changes over longer periods of time.

While a few measurements of F_s and F_e have been made near coastal sites in the Antarctic, little is known about their magnitude elsewhere in the Southern Ocean. Other evidence, however, indicates that turbulent heat transfer is generally more vigorous than in the Arctic and that the turbulent fluxes assume a correspondingly more important role in the heat and mass balance of Antarctic sea ice. An analysis of surface energy fluxes over the ice in the two hemispheres (Andreas and Ackley, 1982) suggests that lower relative humidities and higher average wind speeds in the Antarctic lead to turbulent heat losses which are sufficiently large to inhibit surface melting during the summer. Given a

similar net radiation balance, Andreas and Ackley conclude that air temperatures in the Antarctic must be 2-4°C warmer than in the Arctic before surface melting can be initiated. Differences in surface roughness and cloudiness may also affect the relative importance of F_s and F_e in the two regions, but considerably more data must be acquired in the Antarctic before a final assessment will be possible.

5.2.3 Conductive Heat Flux

Except for the summer melt season, temperatures in the upper part of the ice are colder than those at the underside, causing an upward conduction of heat. The amount of heat reaching the surface depends on the temperature gradient at the surface and the thermal conductivity of the ice (k_i)

$$F_c = k_i \left(\frac{\partial T}{\partial z}\right)_o \quad .$$

In pure ice, the conductivity (k_o) depends on temperature (T) and can be approximated by the relation $k_o = 9.828 \exp(-0.0057T)$, where T is in °K and k_o in W m^{-1} $°K^{-1}$ (Yen, 1981). A typical value for k_o in warm ice is 2.1 W m^{-1} $°K^{-1}$. Heat transport in sea ice is complicated by the presence of brine pockets which decrease its thermal conductivity relative to that of fresh ice. Detailed theories, taking into account the effects of brine pocket distribution, air bubbles, and precipitation of solid salts on k_i, have been worked out (Anderson, 1958; Schwedtfeger, 1963). Untersteiner (1961) found that k_i was directly related to the brine volume and introduced the approximate formula

$$k_i = k_o + \frac{\beta S_i}{T_i} \qquad (5.15)$$

where S_i is the salinity of the ice in ppt, T_i is in °C, and β = 0.13 W m^{-1}. Although somewhat crude, eq. (5.15) is particularly convenient in applications requiring a simple functional relationship between R_i, T_i and S_i. Under natural conditions k_i varies by 10-20% in perennial ice and by up to 50% in young ice. Monthly totals of F_c in perennial ice are remarkably constant between September and April, varying between 30 and 40 MJ m^{-2} mo^{-1} (Maykut and Untersteiner, 1971). This is due to the increasing thickness of the snow cover as temperatures cool during the fall, and to the relatively constant snow depth and temperature averages during the winter.

Except during the melt season there is an upward flux of heat in the ice which supplies much of the energy needed to balance the longwave loss at the surface. Over an annual cycle the amount of heat conducted to the surface of multiyear ice is the sum of the

sensible heat input fr
by bottom accretion, a
in brine pockets and
ice, F_c averages about
ocean, 40% by bottom
the brine pockets and
In young ice, F_c can
than in multiyear ice
season the amount of h
is roughly 2 to 3 times

Because of its low
snow insulates the ice
the ice loses heat dur
dence of F_c on snow dep
a factor of three decr
The rate of decrease in
increases, temperatures
to T_a and more sensiti
ice, producing the de

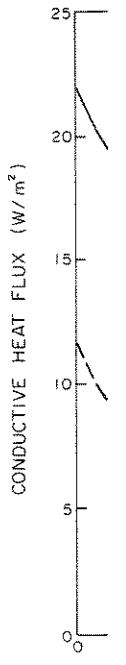

Fig. 9. Effects of sn
perennial ice
and early spri

sensible heat input from the ocean (F_w), the latent heat released by bottom accretion, and the shortwave energy temporarily stored in brine pockets and surface melt ponds. For perennial arctic ice, F_c averages about 8.8 W m^{-2}, of which 20% is supplied by the ocean, 40% by bottom accretion, 30% by release of heat stored in the brine pockets and 10% by the freezing of surface meltwater. In young ice, F_c can be more than two orders of magnitude larger than in multiyear ice. Over the course of the entire growth season the amount of heat conducted to the surface of seasonal ice is roughly 2 to 3 times the annual total for perennial ice.

Because of its low thermal conductivity (k_s = .31 W m^{-1} $^oK^{-1}$), snow insulates the ice from the air, decreasing the rate at which the ice loses heat during the winter. Figure 9 shows the dependence of F_c on snow depth (h_s) in perennial ice. There is roughly a factor of three decrease in F_c as h_s increases from 0 to 100 cm. The rate of decrease in F_c is most rapid when h_s is small. As h_s increases, temperatures in the underlying ice become less sensitive to T_a and more sensitive to the temperature at the bottom of the ice, producing the decreasing effect on F_c with increasing h_s.

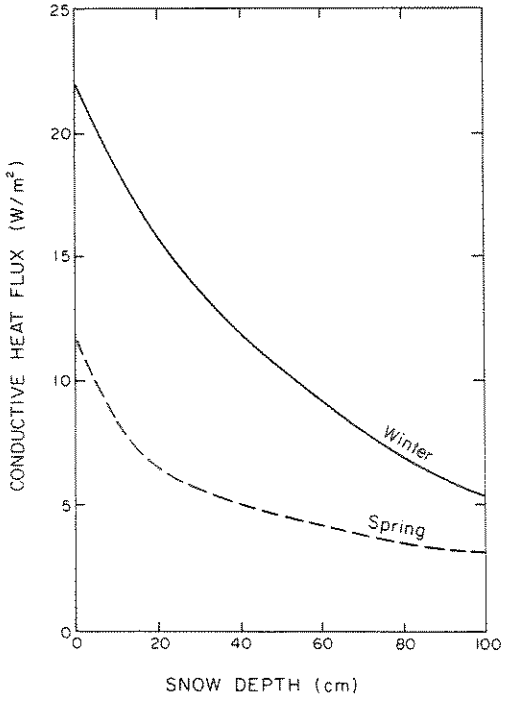

Fig. 9. Effects of snow depth on heat conducted to the surface of perennial ice during mid-winter (solid curve, $\overline{T}_a$ = -34°C) and early spring (dashed curve, $\overline{T}_a$ = -22°C).

Heat conduction through young sea ice (Figure 10) is much more sensitive than the thicker ice to changes in h_s when h_s is small, but is less sensitive when h_s is large. This is because the thermal conductance $[k_i\ k_s/(k_s H + k_i\ h_s)]$ of the combined ice-snow slab is dominated by the properties of te snow cover when the ice is thin (Maykut, 1978). For the cases shown in Figure 10, F_c is essentially constant once h_s exceeds 15-20 cm.

5.2.4 Oceanic Heat Flux

Observations of ablation at the underside of the ice (Badgley, 1966) and theoretical calculations (Untersteiner, 1964; Maykut and Untersteiner, 1971) indicate that there is a net flux of heat from the ocean (F_w) to the underside of the ice on the order of 2 W m^{-2} in the Central Arctic; little is known directly about F_w in areas of seasonal ice. The source of this energy has usually been ascribed to heat advected into the Arctic Ocean from the Atlantic. A relatively warm layer of Atlantic water can be identified throughout much of the central basin. Estimates of the rate of heat loss from the Atlantic layer in the Central Arctic (Panov and Shpaikher, 1964) indicate average rates of 2.0-2.6 W m^{-2}, consistent with the other evidence. Other investigators (Aagaard et al. 1981), however, have suggested that temperature changes in the Atlantic layer are not due to the upward loss of heat to the ice, but rather to mixing with colder shelf water. A more likely source for F_w may thus be shortwave energy which enters the upper ocean through leads. This possibility will be explored in more detail in Section 5.4. The largest values of F_w in the Arctic probably occur in the Fram Strait region where Atlantic water enters the basin and is still close to the surface.

In the Antarctic, surface ablation generally appears to be small (Andreas and Ackley, 1982), indicating that the seasonal disappearance of the ice pack must be caused almost entirely by energy contained in the water. Although shortwave radiation absorbed in the upper ocean must be a major component of F_w there, heat from the deeper ocean also appears to be important. Gordon (1981) estimates that up to 50% of the F_w could be derived from water below the pycnocline, but the uncertainty in this estimate appears to be large.

5.3 ICE GROWTH

5.3.1 General Pattern of Growth and Decay

When discussing ice growth in the polar oceans, it is convenient to consider areas of seasonal and perennial ice separately. Ice in the seasonal sea ice zone (SSIZ) forms in the fall or winter and melts away completely during the following spring and summer. Seasonal sea ice may reach a maximum thickness anywhere from a few

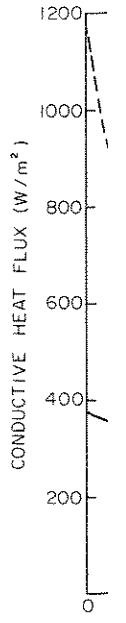

Fig. 10. Effects of
during mid-
10 cm thick

centimeters to a coup
climate is such that
pletely during succe
of ice in the Centr
assumed to be unifor
crease in ice thickn
becomes larger. Eve
negligible and the
environment. Figur
steady climatic con
dependent changes i
approach an equilibr
and advection of ice
ideal from ever beir
numerous heat and mas
the Central Arctic i
ness tends to be som
cussed in Section 5.4

Sea ice extent
Figure 15.1 where we

gure 10) is much more
ı h_s when h_s is small,
This is because the
the combined ice-snow
now cover when the ice
n in Figure 10, F_c is
.

e of the ice (Badgley,
ner, 1964; Maykut and
net flux of heat from
the order of 2 W m^{-2}
tly about F_w in areas
gy has usually been
an from the Atlantic.
can be identified
mates of the rate of
al Arctic (Panov and
0-2.6 W m^{-2}, consist-
tors (Aagaard et al.
ture changes in the
of heat to the ice,
er. A more likely
ich enters the upper
be explored in more
of F_w in the Arctic
here Atlantic water
face.

rally appears to be
at the seasonal dis-
t entirely by energy
diation absorbed in
F_w there, heat from
Gordon (1981) esti-
ed from water below
imate appears to be

eans, it is conven-
ial ice separately.
the fall or winter
spring and summer.
nywhere from a few

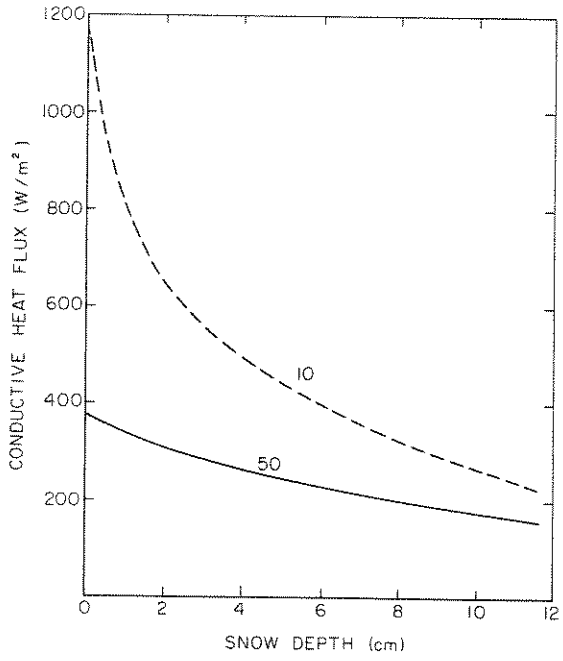

Fig. 10. Effects of snow depth on heat conduction in young ice during mid-winter (T_a = -34°C). The dashed curve shows 10 cm thick ice and the solid curve 50 cm thick ice.

centimeters to a couple of meters. In areas of perennial ice, the climate is such that ice formed during the fall does not melt completely during succeeding summers. Figure 11 follows the growth of ice in the Central Arctic under climatic conditions which are assumed to be uniform from year to year. Note that the net increase in ice thickness slowly decreases as the average thickness becomes larger. Eventually year to year thickness changes become negligible and the ice is said to be in equilibrium with its environment. Figure 12 shows in nomographic form how, under steady climatic conditions and no dynamic motions, thickness dependent changes in ablation and accretion cause the ice to approach an equilibrium thickness (H_e). While changes in climate and advection of ice into different climatic regions prevent this ideal from ever being attained exactly, the concept is useful in numerous heat and mass balance problems. Equilibrium thickness in the Central Arctic is on the order of 3 m, but the average thickness tends to be somewhat larger because of dynamic effects discussed in Section 5.4.

Sea ice extent in the Northern Hemisphere is sketched in Figure 15.1 where we see that most of the Central Arctic Ocean is

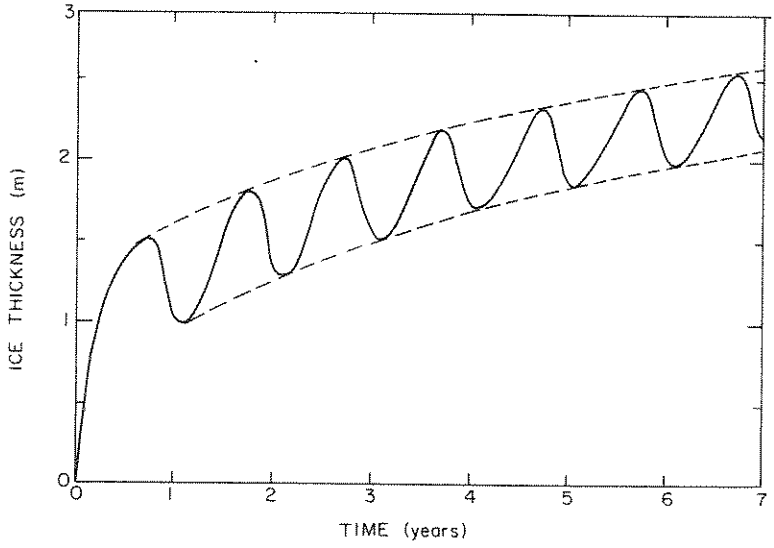

Fig. 11. Pattern of ice growth in the Central Arctic. (After Maykut and Untersteiner, 1971).

covered by perennial ice and most of the peripheral seas by seasonal ice. There have been numerous studies of the formation and growth of young ice in the SSIZ, but most of the work in the Central Arctic has focused on thick multiyear ice. How well ice growth equations derived from observations in the SSIZ describe the growth of young ice in the Central Arctic is not known. Decay of ice in the northern hemisphere SSIZ generally proceeds rapidly following the onset of snow melt. Usually within a week or so shallow meltwater puddles begin to cover the ice and a network of surface drainage canals and vertical melt holes develop. Melt ponds decrease the average surface albedo to as low as 0.4 (Langleben, 1971), greatly increasing the shortwave absorption. In addition, warm winds from nearby land masses often accelerate the surface melting of coastal ice where ablation rates can reach .04 m day^{-1}. At the same time, shortwave radiation absorbed within the salty seasonal ice causes internal melting and structural weakening. Cracking of the weakened ice produces leads which absorb several times as much solar energy as the ice. Heat absorbed in the water causes bottom ablation and lateral melting on the floe edges, increasing the area of open water and forming a positive feedback loop. These processes can result in the complete disappearance of the annual ice cover from sheltered bays and fjords along the arctic coast in a month or less after breakup begins (Langleben, 1972).

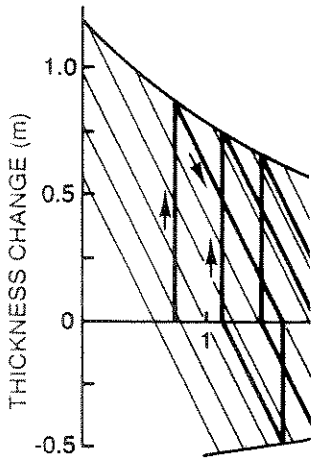

Fig. 12. Nomogram sh
(September–M
ness under
Arctic (afte
er, 1969, 1
thickness (
downward un
is encounte
horizontal
procedure is
examples o
cycles. It
regardless

Similar melt pro
but with less dramati
most of the ice melt t
ing at the upper sur
snow and .4-.5 m of
observed on the under
1965), the situation
which brings about th
at the interface betw
Martin and Kauffman,
of this freshwater on
been made. Enhanced
.1-.4 m to the total
the ponds remaining
absorption in the mel
underlying ice of as

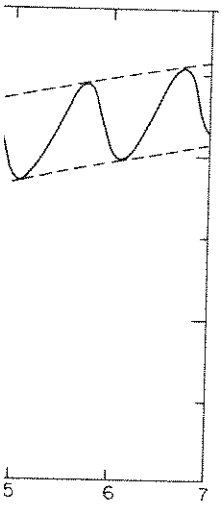

ıral Arctic. (After

ıeral seas by season-
f the formation and
of the work in the
ice. How well ice
ın the SSIZ describe
is not known. Decay
lly proceeds rapidly
vithin a week or so
ice and a network of
ıles develop. Melt
to as low as 0.4
ıortwave absorption.
ses often accelerate
ion rates can reach
radiation absorbed
melting and struc-
ice produces leads
y as the ice. Heat
and lateral melting
water and forming a
result in the com-
rom sheltered bays
less after breakup

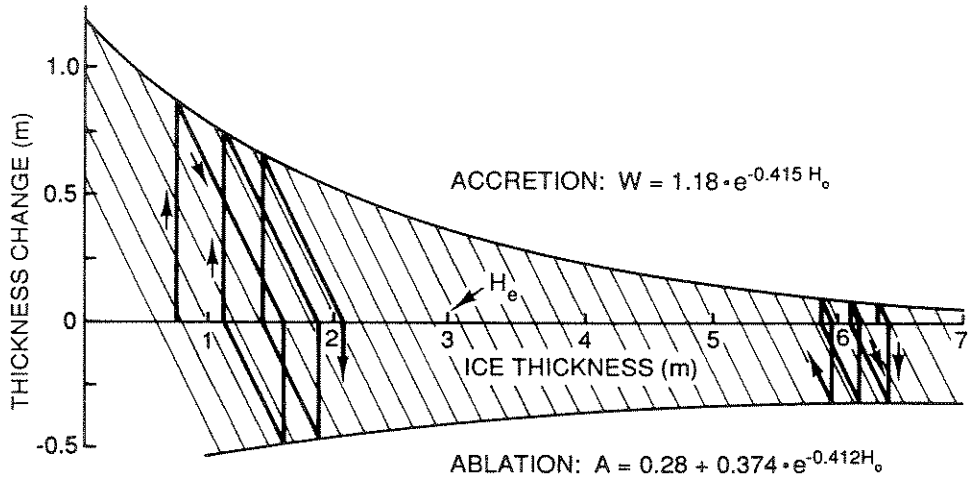

Fig. 12. Nomogram showing the theoretical dependence of accretion (September–May) and ablation (June–August) on ice thickness under present climatic conditions in the Central Arctic (after Untersteiner, 1962; Maykut and Untersteiner, 1969, 1971). Seasonal mass changes for any initial thickness (H_o) are obtained by first moving upward or downward until the accretion (W) or ablation (A) curve is encountered; following the slanted lines back to the horizontal axis then gives the new ice thickness. This procedure is illustrated by the heavy lines which show examples of thickness changes over several annual cycles. It can be seen that ice thickness approaches H_e regardless of whether $H_o < H_e$ or $H_o > H_e$.

Similar melt processes take place in areas of perennial ice, but with less dramatic results. Snow begins melting in June, with most of the ice melt taking place in July and August -- total melting at the upper surface is some 500–600 kg m^{-2}, about .4 m of snow and .4–.5 m of ice. While some melting (.1–.2 m) has been observed on the underside of the ice (Untersteiner, 1961; Hanson, 1965), the situation there is complicated by freshwater runoff which brings about the formation of an ice layer ("false bottom") at the interface between the fresh and salty water (Hanson, 1965; Martin and Kauffman, 1974). Field studies of the overall effects of this freshwater on the mass balance of the ice pack have not been made. Enhanced melting in ponded areas contributes another .3–.4 m to the total mass loss, but part of this is returned when the ponds remaining in the fall refreeze. Strong shortwave absorption in the melt ponds can result in brine volumes in the underlying ice of as high as 50%, compared to maximum values of

about 16% in unponded ice. Typical brine volumes in bare multi-year ice lie in the 8-12% range (Schwarzacher, 1959). Melting of young ice in leads and lateral ablation or erosion from floe edges increase the open water fraction from about 2% in early June to 10-15% in August. Substantial variations in the amount of open water can also be brought about as a result of general divergence or convergence of the region. Once freezeup begins in late August or early September, it takes 3-4 months to cool the ice enough to release all the heat stored in the melt ponds and brine pockets during the summer. As we will show in Section 5.4, freezing of the open water formed during the melt season has an important effect on the overall heat and mass balance of the region.

With the exception of the Weddell Sea, most of the ice in the Southern Ocean is seasonal (Fig. 15.2), however, the decay pattern of this ice appears to be strikingly different from that in the Arctic. Katabatic winds, higher latitudes, and lower oceanic heat fluxes cause melt rates near the continental boundaries to be small compared to those near the free boundary of the Antarctic ice pack. Moreover, the melt ponds which are so characteristic of ice decay in the Arctic have rarely been observed in the Antarctic, and surface melting appears to be minimal. The reason is related to differences in the meteorological variables that control the surface heat balance. Surface melting in the Arctic often takes place with air temperatures significantly below freezing. In the Antarctic, Andreas and Ackley (1982) argue that lower relative humidities and stronger winds enhance turbulent heat losses from the ice and allow surface melting to occur only when air temperatures are above 0 ^{o}C, a condition rarely encountered over the ice cover in the Southern Ocean. Thus, decay and retreat of the Antarctic ice pack are controlled primarily by the rate of heat transfer at the ice-water interface. At this point, there are few details regarding this process.

5.3.2 Young Ice Growth

Empirical Relations. Field studies have shown that the thickness (H) of young sea ice is closely related to the cumulative number of freezing-degree days θ, where

$$\theta \equiv \int_0^t (T_f - T_a)dt \quad ,$$

T_f is the freezing point of the water and T_a is the air temperature at screen height (usually 2 m). Typical results are those obtained by Anderson (1961) near Thule, Greenland (Figure 13). As the ice becomes thicker, the relationship between θ and H becomes weaker, e.g., Anderson observed ice thicknesses varying between 90 and 140 cm for θ = 3000^{o}C day. Although Anderson's data cannot be

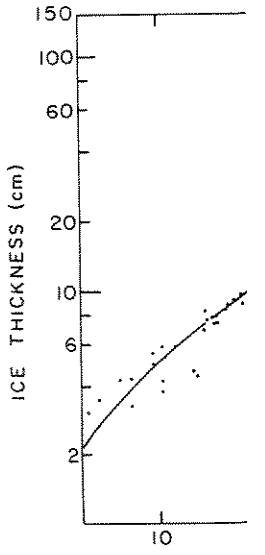

Fig. 13. Relationship
the cumulativ
Anderson, 196

fitted with a simple p
that a good approximati

$$H^2 + 5.1H = 6.7\theta$$

where H is in centimete
Other relationships h
observations near Cape

$$H^2 + 50H = 8\theta$$

and by Lebedev (1938) u
various locations in th

$$H = 1.33\theta^{0.58} \quad .$$

More complex, semi-emp
Lee and Simpson (1954)

According to Ande
or no snow cover, whil
growth under "average"
in location, climate

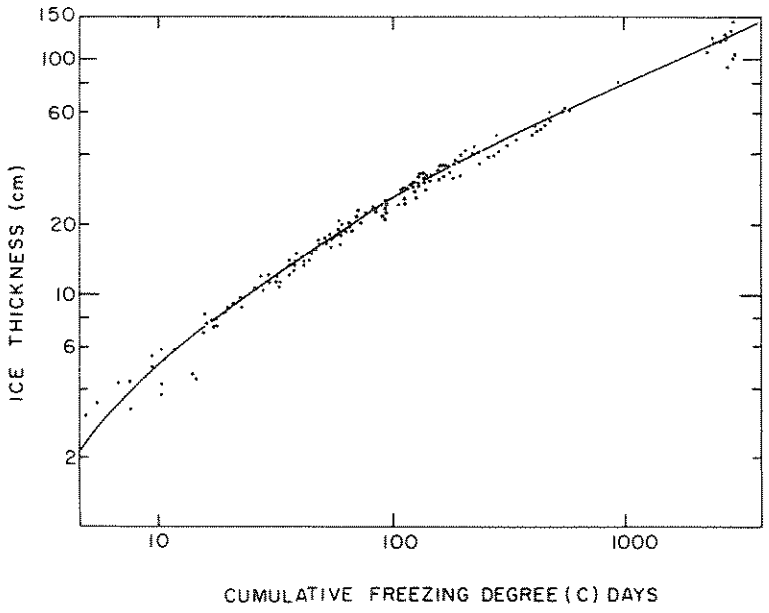

Fig. 13. Relationship between the thickness of young sea ice and the cumulative number of freezing-degree days. (After Anderson, 1961.)

fitted with a simple power law across its entire range, he found that a good approximation was obtained with

$$H^2 + 5.1H = 6.7\theta \qquad (5.16)$$

where H is in centimeters ($10<H<80$ cm) and θ has units of ^{o}C day. Other relationships have been derived by Zubov (1943) from observations near Cape Schmidt

$$H^2 + 50H = 8\theta \qquad (5.17)$$

and by Lebedev (1938) using 24 stations years of observations from various locations in the Soviet Arctic

$$H = 1.33\theta^{.58} \quad . \qquad (5.18)$$

More complex, semi-empirical methods have also been developed by Lee and Simpson (1954) and Bilello (1961).

According to Anderson, eq. (5.16) describes ice with little or no snow cover, while Lebedev states that eq. (5.18) describes growth under "average" snow conditions. Despite the differences in location, climate, and snowfall, eqs. (5.16)-(5.18) are

surprisingly consistent. Figure 14 shows that they generally agree to within about 10 cm. The more rapid growth given by Anderson is to be expected because of the smaller amount of snow. Increasing scatter in the observations at larger H indicate that these equations are valid over a limited thickness range; Anderson's results imply an upper bound of about 1 meter. The closeness of the empirical results suggest that good estimates of H can be obtained without specific knowledge of winds, cloudiness, snowfall, oceanic heat flux, etc. On the other hand, it might be argued that the magnitude of these quantities were similar because the observations were all carried out close to land, or that there were compensating effects (e.g., smaller h_s but larger F_w) which obscured the importance of other factors. Observations taken in conjunction with the ice growth measurements are inadequate to settle such questions.

Results from the above studies demonstrate that the rate of growth of young ice is very sensitive to H. Figure 15 is based on Anderson's data and shows that the growth rate decreases by almost an order of magnitude between H = 10 and H = 100 cm. Effects of differences in air temperature decrease as H increases.

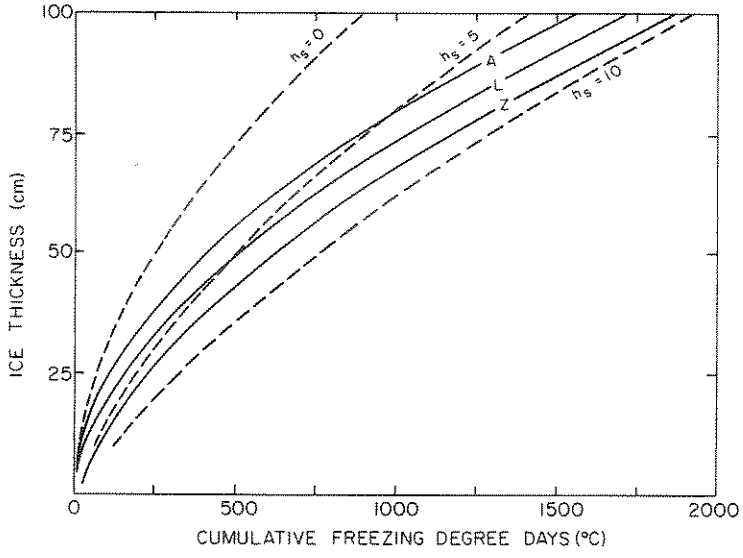

Fig. 14. The solid curves show ice growth predictions by the empirical formulas of Anderson (A), Lebedev (L), and Zubov (Z). Dashed curves show theoretical relationships between ice thickness and degree-days obtained from eq. (5.23) for different thicknesses (h_s) of snow.

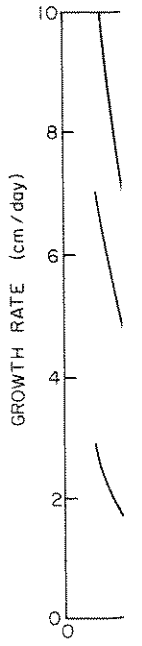

Fig. 15. Dependence of
for air temper

It does not seem l
rate at which sea ice
would be successful. Va
oceanic heat flux, surf
equally important. Hov
near-shore data with the

$$\Delta H = 0.55\theta'$$

where ΔH = the total dec
lated degree-days above
correlation coefficient
cm. Bilello also mer
Karelin for the Soviet A

$$\Delta H = 0.51(\theta'' - 32)$$

where θ'' = the accumula
the correlations found
quent incursions of w

s that they generally
rapid growth given by
smaller amount of snow.
larger H indicate that
ted thickness range;
about 1 meter. The
that good estimates of
of winds, cloudiness,
ther hand, it might be
s were similar because
to land, or that there
but larger F_w) which
Observations taken in
ts are inadequate to

rate that the rate of
Figure 15 is based on
te decreases by almost
= 100 cm. Effects of
increases.

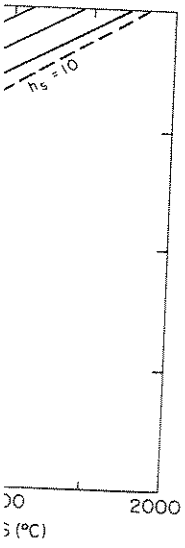

predictions by the
, Lebedev (L), and
etical relationships
s obtained from eq.
of snow.

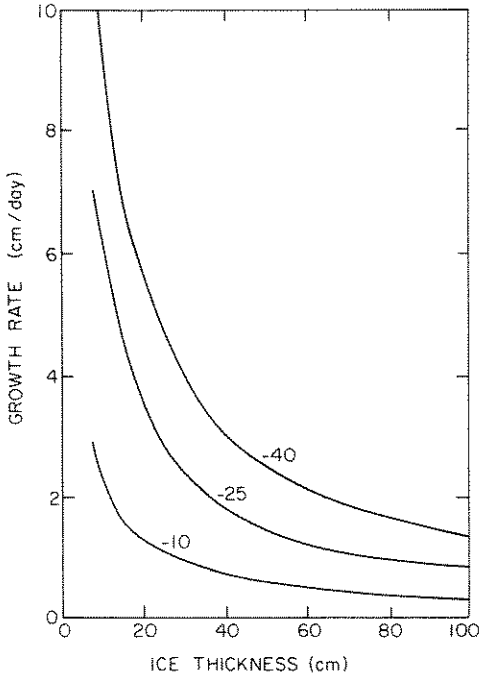

Fig. 15. Dependence of growth rates in young sea ice on thickness for air temperatures of -10, -25, and -40°C.

It does not seem likely that analogous attempts to relate the rate at which sea ice decreases in thickness during the summer would be successful. Variations in cloudiness, area of open water, oceanic heat flux, surface albedo and the like would seem to be equally important. However, Bilello (1961) found a good fit to near-shore data with the equation

$$\Delta H = 0.55\theta'$$

where ΔH = the total decrease in ice thickness and θ' = the accumulated degree-days above T_f. A least squares computation yielded a correlation coefficient of 0.93 and a standard deviation of 16.4 cm. Bilello also mentions another relationship developed by Karelin for the Soviet Arctic

$$\Delta H = 0.51(\theta'' - 32)$$

where θ'' = the accumulated degree days above -5°C. The reason for the correlations found by Bilello and Karelin must be due to frequent incursions of warm air from nearby land masses. It is

doubtful whether such relationships could work away from coastal areas where summer values of T_a are invariably close to 0°C.

Analytical Relations. The strong dependence of H on θ observed in the field can be shown to have a simple physical basis. Let us consider a slab of ice thickness H and conductivity k_i. Temperature at the bottom of the ice is fixed at the freezing point of the water (T_f), while the temperature at the surface (T_o) is free to vary in response to changes in the energy balance. If the ice is thin, the temperature gradient in the ice will be essentially linear and $F_c(z = 0) = F_c(z = H)$ (see Figure 16), hence

$$F_c = \frac{k_i}{H}(T_o - T_f) \quad . \tag{5.19}$$

The amount of growth (or ablation) at the bottom of the ice is determined by the sum of F_w and F_c. If the sum is positive, ice will melt; if the sun is negative, ice will grow, releasing enough latent heat to balance the energy deficit, i.e.

$$-\rho_i L\frac{dH}{dt} = F_c + F_w \quad . \tag{5.20}$$

If we take the simplest possible case where $F_w = 0$ and $T_o = T_a$, eq. (5.20) becomes

$$\rho_i L\frac{dH}{dt} = \frac{k_i}{H}(T_f - T_a) \quad .$$

Assuming that H(t=0)=0, integration of this equation gives

$$H^2 = \frac{2k_i}{\rho_i L}\int_o^t (T_f - T_a)dt = \frac{2k_i}{\rho_i L}\theta \quad .$$

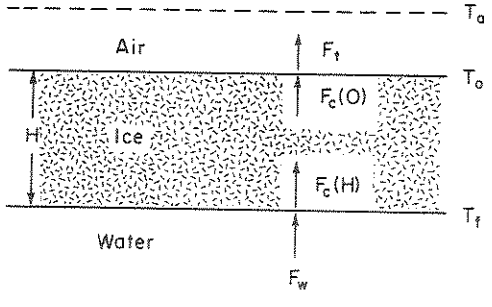

Fig. 16. Idealized picture of the ice slab and heat fluxes.

This equation is u
when H is small. T
and Zubov, we must
will assume that the
atmosphere (F_t) is
T_a, i.e.,

$$F_t = C_t(T_a - T_c$$

where C_t is some
describes both sens
the upper surface m

$$\frac{k_i}{H}(T_o - T_f) = ($$

Solving this equatic

$$T_o = \frac{k_i T_f + C_t H}{k_i + C_t H}$$

Substituting eq. (5.

$$F_c = \frac{k_i C_t}{k_i + C_t H} ($$

Again assuming that
(5.20) now yields

$$H^2 + \frac{2k_i}{C_t} H = \frac{2k}{\rho_i}$$

How well does this e
cal cm^{-1} day^{-1} $°C^{-1}$
sensible heat flux a
= 65 cal cm^{-3} (cor
eq. (5.22) becomes

$$H^2 + 16.8H = 12$$

which is graphed in
clearly predicts muc
One possible reason
include a snow laye
flux in the snow mu
forward to show that

ork away from coastal
r close to 0°C.

idence of H on θ ob-
imple physical basis.
and conductivity k_i.
ixed at the freezing
e at the surface (T_o)
energy balance. If
he ice will be essen-
igure 16), hence

(5.19)

ottom of the ice is
sum is positive, ice
ow, releasing enough
.

(5.20)

$_w$ = 0 and $T_o = T_a$,

uation gives

$- T_o$

$- T_o$

$- T_f$

and heat fluxes.

This equation is unrealistic since T_o can be much warmer than T_a when H is small. To obtain the dependence on H noted by Anderson and Zubov, we must relax the assumption that $T_o = T_a$. Instead we will assume that the net rate of heat exchange between the ice and atmosphere (F_t) is proportional to the difference between T_o and T_a, i.e.,

$$F_t = C_t(T_a - T_o)$$

where C_t is some sort of an average transfer coefficient which describes both sensible and latent heat exchange. Heat gain at the upper surface must equal heat loss, so $F_c = F_t$ and

$$\frac{k_i}{H}(T_o - T_f) = C_t(T_a - T_o) \quad .$$

Solving this equation for T_o gives

$$T_o = \frac{k_i T_f + C_t H T_a}{k_i + C_t H} \tag{5.21}$$

Substituting eq. (5.21) into eq. (5.19) gives

$$F_c = \frac{k_i C_t}{k_i + C_t H}(T_f - T_a) \quad .$$

Again assuming that $F_w << F_c$ and H(t=0)=0, integration of eq. (5.20) now yields

$$H^2 + \frac{2k_i}{C_t} H = \frac{2k_i}{\rho_i L} \theta \quad . \tag{5.22}$$

How well does this equation fit the observations? Letting C_t = 50 cal cm^{-1} day^{-1} $^oC^{-1}$ (slightly higher than the nominal value for sensible heat flux alone), k_i = 419.9 cal cm^{-1} day^{-1} $^oC^{-1}$, and $\rho_i L$ = 65 cal cm^{-3} (corresponding to an average brine volume of 10%, eq. (5.22) becomes

$$H^2 + 16.8H = 12.9\theta$$

which is graphed in Figure 14 as the h_s = 0 curve. Equation (5.22) clearly predicts much more rapid growth than observed in nature. One possible reason for this is neglect of the snow cover. If we include a snow layer of depth h_s and specify that the conductive flux in the snow must be equal to that in the ice, it is straightforward to show that

$$H^2 + \left[\frac{2k_i}{k_s} h_s + \frac{2k_i}{C_t}\right] H = \frac{2k_i}{\rho_i L} \theta \qquad (5.23)$$

or

$$H^2 + (13.1\, h_s + 16.8)H = 12.9\theta \ .$$

When $h_s = 0$, the linear term in eq. (5.23) rapidly decreases in importance once H exceeds about 20 cm, so that H becomes increasingly a function of $\theta^{1/2}$. A small amount of snow, however, magnifies the importance of the linear term. For example, when $h_s = 5$ cm, the linear term dominates the expression until H reaches about 75 cm. A few cm of snow also acts to decrease the importance of temperature differences between the air and the surface. Equation (5.23) is graphed in Figure 14 for snow depths of 5 and 10 cm. At first glance it appears that choosing h_s in the 5-10 cm range produces reasonable agreement with the empirical results. This apparent agreement is somewhat deceptive, however, because the good fit at larger H can only be obtained by seriously underestimating growth rates in the thin ice. The problem is with the assumption of a constant h_s. By imposing a layer of snow on the very thin ice, we cause an unrealistic decrease in its rate of growth. It is possible to take into account changes in h_s by stepwise integration of eq. (5.20). This was the approach taken by Nakawo and Sinha (1981) in analyzing ice growth data from Pond Inlet. They found, however, that growth predictions made by including observed variations in h_s were less accurate than those obtained assuming a large constant snow depth. They attributed the apparent failure of the more rigorous method to changes in the physical properties of the growing ice and to uncertainties in the snowfall when the ice was very thin. A more likely explanation is that heat input from the ocean was responsible for the slower than expected growth. Calculations by Lee and Simpson (1954) indicate that at least 40-80 MJ m^{-2} are released from the upper ocean in the SSIZ during the fall and winter, following the initial formation of the ice cover. Allison (1981) infers F_w values beneath seasonal ice near Mawson, Antarctica of 40-120 MJ m^{-2} mo^{-1} (15-50 W m^{-2}) during the first month of growth, dropping to 20-40 MJ m^{-2} mo^{-1} (7-15 W m^{-2}) in succeeding months. Analysis of the Anderson data indicate that an eventual snow accumulation of 15-20 cm is needed to explain differences between observations and theoretical predictions. Since there was actually very little snow, the most likely explanation for the slower growth is again a substantial F_w. This implies that, to be generally applicable, our analytical ice growth formula needs a term describing the effect of F_w on H. Although eq. (5.20) can be solved in some special cases for $F_w \neq 0$, more general solutions require numerical treatment.

Numerical Modelin
given by Anderson and
$F_w(t)$ and $h_s(t)$. As w
tities can have a large
θ. Application of s
ocean heat flux or snow
Southern Ocean) is thu
tions for these areas
directly from ice gr
balance data and theore
shall discuss below.

Let us consider a
by a layer of snow of t
face is in thermal equi
by heat loss. We car
boundary

$$(1 - \alpha)F_r - I_o + F$$

where F_m is the heat l

$$F_m = [\rho L \frac{d(H + h_s}{dt}$$

When the surface tempe
at the melting point,
face will be balanced
are considering the c
perature gradients in

$$F_c = \frac{k_i k_s}{k_i h_s + k_s H} ($$

where γ is the therma
Substituting eqs. (5.1
into eq. (5.24), the u

$$(1 - \alpha)(1 - i_o)F_r$$

$$+ K_e(re_{sa} - e_{so})$$

where $K_s = \rho_a C_p C_s u$ an
cold, thin ice increa
ing spring ice formati
An approximate relatio